Biophysical Journal Volume 105 August 2013 1057–1066

Ultrasensitivity by Molecular Titration in Spatially Propagating Enzymatic Reactions

Sergey N. Semenov,[†] Albert J. Markvoort,[‡§] Wouter B. L. Gevers,[‡§] Aigars Piruska,[†] Tom F. A. de Greef,[‡§*] and Wilhelm T. S. Huck[†*]

[†]Radboud University Nijmegen, Institute for Molecules and Materials, Nijmegen, The Netherlands; [‡]Eindhoven University of Technology, Institute for Complex Molecular Systems and [§]Computational Biology Group, Eindhoven, The Netherlands

ABSTRACT Delineating design principles of biological systems by reconstitution of purified components offers a platform to gauge the influence of critical physicochemical parameters on minimal biological systems of reduced complexity. Here we unravel the effect of strong reversible inhibitors on the spatiotemporal propagation of enzymatic reactions in a confined environment in vitro. We use micropatterned, enzyme-laden agarose gels which are stamped on polyacrylamide films containing immobilized substrates and reversible inhibitors. Quantitative fluorescence imaging combined with detailed numerical simulations of the reaction-diffusion process reveal that a shallow gradient of enzyme is converted into a steep product gradient by addition of strong inhibitors, consistent with a mathematical model of molecular titration. The results confirm that ultrasensitive and threshold effects at the molecular level can convert a graded input signal to a steep spatial response at macroscopic length scales.

INTRODUCTION

The rapid progress in synthetic biology (1–3) has stimulated research into reconstituted minimal biological systems that display complex spatiotemporal behavior (4–8). Central to this bottom-up strategy is the fundamental understanding of important biological design rules critical to a specific cellular function, constructed from a minimal set of components. These efforts necessarily involve replacing the complex and idiosyncratic biochemical networks encountered in the cell with simpler and more predictable molecular circuitry in vitro. In the last decade, this approach has resulted in in vitro model systems that have contributed to our understanding of basic design principles of biochemical circuits. Examples include engineered DNA circuits capable of bistable (9,10) or oscillatory (11–13) dynamics, and purified biochemical systems displaying spatiotemporal pattern formation (14–17). Spatiotemporal pattern formation arising via coupling of reaction and diffusion is increasingly recognized as an important driving force for intra- and intercellular organization (18–21). A unified view is emerging in which spatial organization in cellular systems arises from the dynamic interaction of molecular gradients and signaling cascades influenced by cell shape (22), feedback loops (23), differential diffusivity of molecules (24), and ultrasensitive threshold responses (25,26).

Ultrasensitive or all-or-none input/output responses play an important role in many intra- and intercellular processes by providing a mechanism that allows switching between two functional states upon crossing a threshold. Close to the threshold, a small change in one parameter results in a steep response in the output. Biochemical signal amplification necessary for generating such switchlike behavior can arise via allosteric cooperative interactions between proteins (27), but various noncooperative mechanisms have been identified that also allow for an ultrasensitive input/output response. For example, covalent modification of substrates by futile cycles of competing enzymes can result in sharp, switchlike responses (25,28,29). Stoichiometric sequestration (i.e., molecular titration) offers an alternative and highly tunable mechanism for signal amplification and threshold setting which does not make use of competing enzyme pairs (26,30–32). Molecular titration occurs when active components, for example, enzymes, transcription factors, or mRNAs, are stoichiometrically sequestered by reversible binding to (macromolecular) inhibitors. In the case of enzymatic reactions, competitive inhibitors can act as a buffering sink, and only when the total enzyme concentration is raised does the inhibitor sink eventually saturate, leading to a steep increase in free, active enzyme. It has been suggested that when coupled to diffusion, ultrasensitive switches, generated by either covalent modification (33) or molecular titration (34), are an important mechanism by which a continuous, shallow gradient of a morphogen can be converted into a steep gradient of a downstream effector necessary for spatially controlled gene expression. However, these studies have remained largely theoretical and no systematic experimental study on the effect of molecular titration in an engineered in vitro system has been reported to our knowledge. Here, we describe the successful in vitro reconstitution of a simple biochemical model system that shows the influence of ultrasensitive and threshold effects on spatial propagation of enzymatic activity in a confined environment. Although ours is a model system where the substrate is immobilized, the results are relevant for biochemical reaction networks in which the substrate has a higher molecular weight compared to the inhibitor, as is the case in regulation of mRNA expression levels by microRNAs (35).

Submitted May 7, 2013, and accepted for publication July 1, 2013.

*Correspondence: t.f.a.d.greef@tue.nl or w.huck@science.ru.nl

Editor: Stanislav Shvartsman.

0006-3495/13/08/1057/10 $2.00

http://dx.doi.org/10.1016/j.bpj.2013.07.002

METHODS

Synthesis of substrate functionalized polyacrylamide hydrogels

Substrate functionalized polyacrylamide (PAAm) hydrogels were prepared according to a procedure described in the literature (36). Prepolymer solution containing acrylamide (9.7%), bis-acrylamide (0.4%), and required amounts of acrylamide functionalized fluorogenic substrate (*S*) was casted between two hydrophobic glass slides separated by a thin spacer (1.0 or 0.4 mm). The *N*-acryloyl-ε-aminohexanoic-acid-modified soybean trypsin inhibitor (STI) was added to the prepolymer solution to obtain STI-modified gels. Polymerization was initiated using ammonium persulfate (APS) and tetramethylethylenediamine (TEMED). Hydrogels were stored in 10 mM Tris buffer (pH 7.8). The rhodamine-110-based fluorogenic substrate was obtained by stepwise functionalization of amino residues with acryloyl β-alanine and Nα-acetyl lysine using 1-ethyl-3-(3-dimethylaminopropyl)carbodiimide coupling. Detailed synthetic protocols and analytical data of the synthetized compounds are available in Section 1 of the Supporting Material.

WET stamping, data collection, and data treatment

The modified wet stamping procedure reported by Grzybowski et al. was used (36). A functionalized PAAm gel stamp (1 × 1.5 cm) was soaked in 10 mM Tris buffer (pH 7.8) containing an appropriate amount of the inhibitor and equilibrated in solution for at least 12 h. A 6% agarose stamp was soaked in a trypsin solution for at least 15 h at 4°C. Then the piece of PAAm gel was placed on the glass slides and dried for 30 s (care was taken to prevent formation of air bubbles between the glass slide and the gel.) The agarose stamp was brought in contact (feature side down) with the PAAm gel. The obtained construct was covered by a plastic cup containing a piece of wet cotton to prevent drying during an experiment and was placed on the microscope stage. The contact of the stamp pillars with the PAAm gel was brought into focus and a series of fluorescent images were acquired. All experiments were performed on an inverted epifluorescence microscope (IX81, Olympus, Center Valley, PA) equipped with a high-pressure mercury lamp (Olympus), a U-FGFP filter cube (Olympus), an iXon 897 camera (Andor, Belfast, United Kingdom), and a 2× objective (Plan, 0.06 NA, Olympus).

Kymograph construction consisted of the following steps. At first, background correction parameters were determined for each set of images. Next, a profile along the *x* axis (Fig. 1 *a*) with a width of 200 μm in the *y* direction was extracted for each time point and a background correction was applied. Finally, intensity profiles were assembled into an (*x*,*t*) kymograph. Further details of the procedure and the ImageJ macro are available in Section 2 of the Supporting Material.

Computational model and kymographs

Partial differential equations (PDEs) were numerically solved using custom-written scripts in Matlab on the appropriate 2D geometry (Fig. S16 in the Supporting Material). A time-splitting, finite-difference algorithm is employed in which concentrations in time and space are updated in two separate steps reflecting the different timescales of the various processes, i.e., 1), equilibration of enzyme-substrate and enzyme-inhibitor complexes, and 2), diffusion of free enzyme, free noncross-linked inhibitor, and enzyme-inhibitor species and simultaneous conversion of enzyme-substrate complex into fluorescent product.

Complexation

Because protein-substrate and protein-inhibitor association kinetics are fast ($k_f > 10^4\ M^{-1}\ s^{-1}$) compared to diffusion of proteins and inhibitors ($D < 10^{-11}\ m^2\ s^{-1}$) and catalytic conversion of enzyme-substrate complex ($0.1\ s^{-1} < k_{cat} < 100\ s^{-1}$), a pseudo-steady-state approximation can be employed. In this step, concentrations are updated instantaneously with respect to diffusion and conversion by solving the equilibrium and mass-balance relations. Equilibration of enzyme-substrate (with dissociation constant K_d) is taken into account by solving a second-order algebraic equation at each spatial point on the grid (36). Instantaneous equilibration of enzyme-substrate and enzyme-inhibitor complexes (with dissociation constants K_d and K_i, respectively) occurs by solving a third-order algebraic equation at each spatial point on the grid, thus taking into account competition between substrate and inhibitor for binding to the enzyme (37).

Diffusion and conversion

In the second step, the concentration change of species as a result of diffusion (enzyme, noncross-linked inhibitor, and enzyme-inhibitor complexes) or catalytic conversion (enzyme, enzyme-substrate complex, and product) are updated. The diffusion operator is discretized using a second-order accurate alternating-direction implicit (ADI) version of the Crank-Nicholson algorithm or a first-order accurate ADI version of the forward-time central-space (FTCS) scheme. In the algorithm employing the FTCS scheme, discretization of space and time satisfies the stability criterion. The diffusion constants of the STI inhibitor and trypsin-STI complex were determined from the molecular weights of STI and trypsin and the estimated diffusion constant of trypsin obtained by fitting of the kymograph displayed in Fig. 1 *d* ($S = 0.1$ mg/ml). Assuming that the protein, inhibitor, and protein-inhibitor complex have a spherical geometry, the Stokes-Einstein relation shows that the unknown diffusion constant can be estimated as

$$D_{(e)i} = D_e \left(\frac{M_e}{M_{(e)i}} \right)^{\frac{1}{3}}, \tag{1}$$

with M_e the known molecular weight of trypsin, $M_{(e)i}$ the known molecular weight of inhibitor or trypsin-inhibitor complex, and $D_{(e)i}$ the unknown diffusion constant of the inhibitor or trypsin-inhibitor complex.

Because the reaction terms describing catalytic conversion of enzyme-substrate complex are linear, the amount of enzyme-substrate complex that is converted to product and enzyme during a time step can be determined by integrating the ordinary differential equation

$$\frac{\partial [ES]}{\partial t} = -\frac{\partial [P]}{\partial t} = -k_{cat}[ES]. \tag{2}$$

The concentration of product was converted to fluorescence intensity by taking into account absorption of excitation light and emitted fluorescence by covalently bound substrate. To convert the concentration of product to fluorescence intensity, the PAAm gel was divided into a number of layers in the *z* direction with a width equal to the grid size. Within each layer, the excitation and fluorescence emission intensity was calculated using the absorption coefficients at the excitation and emission wavelength. Finally, the total fluorescence intensity was obtained by summing the emission intensity of all layers in the *z* direction. Further details of this procedure can be found in Section 3 of the Supporting Material.

The accuracy of our algorithm was validated by comparing the normalized, absorbance-corrected computed kymograph reported in Fig. 1 *d* (diffusion of trypsin into substrate-laden gels, $[S_0] = 0.1$ mg/ml) to a theoretical kymograph produced by a commercial finite-element code (COMSOL) that solves the full system of PDEs (Eq. 4) without a pseudo-steady-state approximation. The analysis shows that our algorithm performs accurately (1–5% difference in absolute intensity; see Fig. S17) at only a fraction of the total computation cost as long as $k_f >> D_e$, $k_b \geq D_e$, and $k_f >> k_{cat}$. Because forward rate constants of protein-substrate associations are typically on the order of $10^5\ M^{-1}\ s^{-1}$ and the catalytic rate constant, k_{cat}, for β-trypsin (38) is typically on the order of 0.1–100 s^{-1}, it is therefore concluded that the pseudo-steady-state approximation is valid. A similar analysis was performed by comparing the normalized, absorbance-corrected computed kymograph (see Fig. 3 *b*; $[I_0] = 10\ \mu M$) to theoretical kymographs

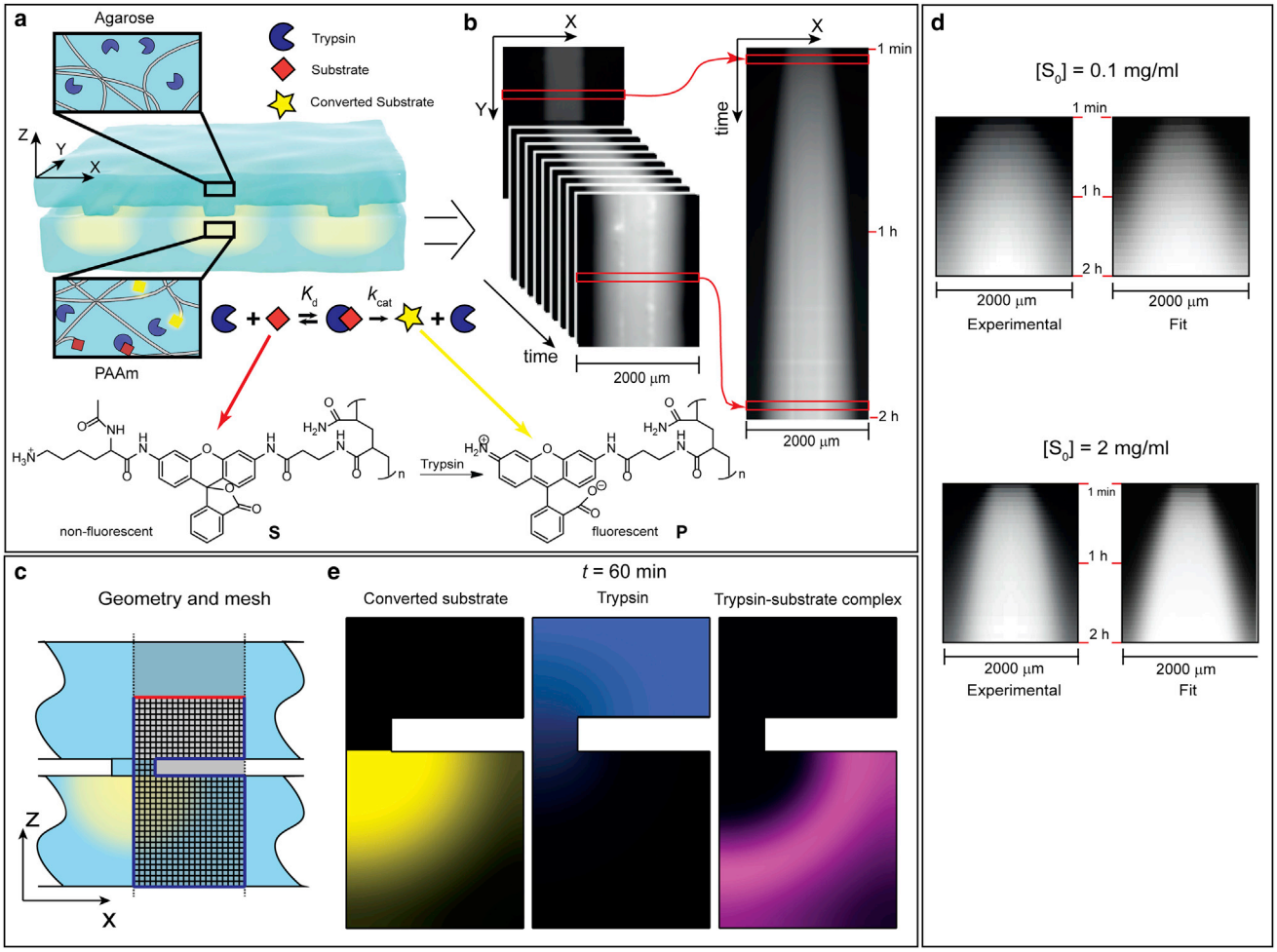

FIGURE 1 Spatial propagation of enzymatic activity. (*a*) Schematic description of the wet stamping (36) experiment. The upper stamp consists of parallel lines (500 μm wide and spaced by 1500 μm) fabricated by casting a hot 6% w/v agarose solution against an oxidized polydimethylsiloxane master. The stamps are then soaked in a trypsin solution ($[E_0] = 1$ mg/ml) at 4°C until saturated with the enzyme. The bottom gel consists of cross-linked PAAm to which a fluorogenic rhodamine substrate is covalently attached. The converted substrate is excited at 455 nm, and fluorescence of the product is measured from the bottom of the gel. (*b*) Processing of the experimental data. Horizontal cross sections from each experimental micrograph in time (*left*) are averaged in the y direction (200 μm) and assembled into a kymograph (*right*). Experimental and computed kymographs were normalized with respect to the highest-intensity value. (*c*) Two-dimensional geometry and boundary conditions used in the numerical model. Blue line shows Neumann boundary conditions; red line shows the Dirichlet boundary condition. (*d*) Parameter estimation by nonlinear least-square minimization of the difference between experimental and computed kymographs. (*Upper*) Total substrate concentration, $[S_0] = 0.1$ mg/ml; total trypsin concentration, $[E_0] = 1$ mg/ml); values of estimated parameters, $D_e = 3.5 \times 10^{-11}$ m^2 s^{-1}, $k_{cat}/K_d = 2.4 \times 10^2$ s^{-1} M^{-1}. (*Lower*) $[S_0] = 2$ mg/ml; $[E_0] = 1$ mg/ml); $D_e = 0.94 \times 10^{-11}$ m^2 s^{-1} and $k_{cat}/K_d = 4.6 \times 10^1$ s^{-1} M^{-1}. (*e*) Computed concentrations of fluorescent product (P), free trypsin (E), and trypsin-substrate complex (ES) in the agarose stamp and PAAm gel obtained using the estimated parameters ($[S_0] = 0.1$ mg/ml, $[E_0] = 1$ mg/ml) at time $t = 60$ min. Although the spatial distribution of product can be calculated using the estimated parameters k_{cat}/K_d and D_e, the concentration of enzyme-substrate complex and free enzyme can only be determined using individual values for k_{cat} and K_d. Literature analysis (38) shows that typical k_{cat} values for β-trypsin fall in the range 0.1–100 s^{-1}, and therefore, an intermediate value of 10 s^{-1} was used in the simulations. As can be observed from the calculated concentration profiles, the product propagates as a moving front while the transient nature of the enzyme-substrate complex results in a broad traveling wave.

produced by a commercial finite-element code (COMSOL) that solves the full system of PDEs (Eq. 5) without a pseudo-steady-state approximation. The results show that the steady-state approximation, in which both the differential equations for association and dissociation of enzyme with substrate and inhibitor, respectively, are replaced by an algebraic equation, is valid.

Nonlinear least-square minimization

Parameter estimation was performed by comparing normalized theoretical and experimental kymographs. Normalized kymographs were obtained by linearly scaling the experimental and computed kymographs between 0 and 1 using the lowest- and highest-intensity values, respectively. Estimated parameters were obtained using the following iterative procedure:

1. Computation of a theoretical, normalized kymograph for an initial set of parameter values.
2. Evaluation of the cost function, a measure of the difference between the normalized experimental and theoretical kymographs.
3. Generation of new parameter values using an optimization algorithm with the goal of minimizing the cost function.

The cost function was defined as the sum of the mean-square difference in each time point between the experimental and simulated kymographs:

$$\chi^2 = \sum_{i,j} \left(I_{\mathrm{mod}}(i,j) - I_{\mathrm{exp}}(i,j)\right)^2, \quad (3)$$

where $I(i,j)$ corresponds to the normalized fluorescence intensity at pixel i,j. Optimization was performed using the Matlab function lsqnonlin, a subspace trust-region method based on the interior-reflective Newton method. The lower bounds of the 95% confidence intervals and asymptotic standard errors were determined using the observed Fisher information matrix (39).

RESULTS AND DISCUSSION

Experimental platform and validation of computational approach

Detection of enzymatic activity with good spatial and temporal resolution is a key issue for the quantitative study of biochemical reaction-diffusion processes. To address this challenge, we designed a PAAm hydrogel with covalently cross-linked fluorogenic substrate (Fig. 1 *a*) (see Supporting Material for experimental details). The fluorogenic substrate becomes fluorescent upon cleavage of a functional group by an enzyme (vide infra) and remains covalently attached to the gel, which allows the position of the product to be probed in space and time (Fig. 1 *a*). The absence of diffusion of the product is key to the design of our experimental system: the fluorescence signal is a direct measurement of the diffusion of the active enzyme through the gel, and this allows us to construct a model where the concentration of all species can be traced in space and time as discussed below.

As a model enzyme, the serine protease β-trypsin was selected because of the availability of various competitive inhibitors (40) and the ease with which enzymatic activity can be probed using fluorogenic substrates (41,42). Although β-trypsin can lose activity by autolysis, this process is very slow at room temperature and the low concentrations used (43). First, we studied spatial propagation of enzymatic activity in the absence of inhibitor, corresponding to a situation in which threshold and ultrasensitive effects are absent at the molecular level. Inspired by the work of Grzybowski and co-workers (36), trypsin was delivered to 1-mm-thick PAAm gels containing cross-linked fluorogenic substrate (S) by wet stamping (44) from micropatterned agarose stamps soaked with a solution of enzyme ($[E_0] = 1$ mg/ml, Fig. 1 *a*). During wet stamping, the micropatterned agarose stamp is brought into conformal contact with the substrate-functionalized PAAm gel, allowing the enzyme to diffuse into the gel. Spatiotemporal product (P) conversion in the PAAm gel was probed using fluorescence microscopy, and time-dependent 2D micrographs were converted to normalized (x,t) kymographs (Fig. 1 *b* and Methods). Quantitative analysis of the data is performed using a numerical model that solves the corresponding system of PDEs on the representative 2D geometry using the appropriate boundary conditions (Fig. 1 *c*) and initial concentrations corresponding to the experimental system:

$$\begin{aligned}
\frac{\partial[S]}{\partial t} &= k_{\mathrm{b}}[ES] - k_{\mathrm{f}}[S][E] \\
\frac{\partial[ES]}{\partial t} &= k_{\mathrm{f}}[S][E] - k_{\mathrm{b}}[ES] - k_{\mathrm{cat}}[ES] \\
\frac{\partial[E]}{\partial t} &= D_{\mathrm{e}}\nabla^2[E] + k_{\mathrm{b}}[ES] - k_{\mathrm{f}}[S][E] + k_{\mathrm{cat}}[ES] \\
\frac{\partial[P]}{\partial t} &= k_{\mathrm{cat}}[ES],
\end{aligned} \quad (4)$$

where D_{e} is the diffusion constant of the enzyme, k_{f} and k_{b} are the forward and backward rate constants, respectively, of enzyme-substrate (ES) association and dissociation, and k_{cat} is the catalytic rate constant of the enzyme (E). Because binding of trypsin to its substrate is much faster than diffusion of the enzyme, a pseudo-steady-state approximation is used in which the ordinary differential equations describing enzyme-substrate association and dissociation are replaced with algebraic equations reflecting rapid equilibrium of enzyme-substrate binding, characterized by the dissociation constant K_{d} ($k_{\mathrm{b}}/k_{\mathrm{f}}$). Comparison of the concentrations obtained from the approximated model with the full PDE model (Eq. 4) shows excellent correspondence at only a fraction of the computational cost (see Methods). Computational kymographs were generated taking into account absorption of excitation light and emitted fluorescence inside the PAAm gel (see Methods). The divergent shape of the experimental kymographs (Fig. 1 *d*) at both substrate concentrations ($[S_0] = 0.1$ and 2 mg/ml) is indicative of conversion of covalently bound substrate by diffusive spreading of the enzyme into the PAAm gel. To validate the computational model and obtain estimates of the parameters that influence spatial propagation of enzymatic activity (K_{d}, k_{cat}, and D_{e}), nonlinear least-square analysis of the normalized experimental and computed kymographs is performed. Fig. 1 *d* shows that although the residual plots (Fig. S3) show some spatiotemporal structure, the computational model describes the experimental kymographs at both substrate concentrations. Analysis of the residual squared-error contours (Fig. S4) and profile-likelihood (45) plots (Fig. S5) reveal that the parameters K_{d} and k_{cat} are correlated at low concentrations of substrate. However, the ratio $k_{\mathrm{cat}}/K_{\mathrm{d}}$, and the diffusion constant D_{e} could be estimated accurately from the experimental kymographs (Table S1).

Next, the spatial distribution of fluorescent product, free enzyme, and enzyme-substrate complex inside the stamp at the lowest substrate concentration (0.1 mg/ml) was computed at $t = 60$ min (Fig. 1 *e*). The analysis shows that starting from the initial condition, where enzyme is only present in the stamp, enzyme diffuses into the PAAm film containing fluorogenic substrate, thereby converting substrate along a propagating front and leaving fluorescent product in its

wake. The propagating front is preceded by a broad traveling wave of enzyme-substrate complex that overlaps considerably with regions of low substrate conversion. Further computational analysis (Figs. S6 and S7) reveals that the steepness of the product front depends mostly on the diffusion constant, whereas the width of the enzyme-substrate wave is independent of the precise value of k_{cat} and K_d over a wide range of realistic parameter values.

Molecular titration and spatial propagation of enzymatic activity

Fig. 2, *a–d*, shows the effect of molecular titration on the steady-state concentration of enzyme-substrate complex for various total concentrations of inhibitor ($[I_0]$) and inhibitor dissociation constants (K_i) calculated using an equilibrium model that takes into account reversible competition between substrate and inhibitor for the same binding site (37). When binding of the enzyme to the inhibitor is much stronger than binding of the enzyme to its substrate, the concentration of enzyme-substrate complex increases sharply above a threshold concentration. It is important to note that both the threshold concentration and sharpness of the response can be tuned by the concentration and dissociation constant of the inhibitor (Fig. 2, *c* and *d*). In our experiments, we study a heterogeneous environment where titration is achieved by diffusion of enzyme into the inhibitor-laden gel from a localized source. In such a case, molecular titration is expected to convert a graded spatial gradient in enzyme concentration into sharp borders of enzymatic activity (Fig. 2 *e*).

Fig. 3 *a* shows the experimental setup in which trypsin at a concentration of 2 mg/ml is delivered to a PAAm gel containing cross-linked fluorogenic substrate ($[S_0]$ = 0.1 mg/ml) and various concentrations of cross-linked STI ($[I_0]$ = 0, 2.5, and 10 μM)).

STI is a strong, reversible inhibitor that binds to trypsin with diffusion-controlled kinetics ($k_f^I \sim 10^8$ M^{-1} s^{-1}) (46–48) and an apparent dissociation constant (K_i) of 10^{-9} M (47). In the presence of cross-linked inhibitor, spatial propagation of enzymatic activity in the PAAm gel is delayed, as is evident from the significant narrowing of the kymographs with increasing concentration of covalent inhibitor (Fig. 3 *b*). We extended the computational model to take into account threshold and ultrasensitive effects arising via competition of inhibitor with substrate for free enzyme by adding terms for the free inhibitor and the inhibitor-enzyme complex. The full PDE model of the system is written as

$$\begin{aligned}
\frac{\partial[S]}{\partial t} &= k_b[ES] - k_f[S][E] \\
\frac{\partial[ES]}{\partial t} &= k_f[S][E] - k_b[ES] - k_{cat}[ES] \\
\frac{\partial[E]}{\partial t} &= D_e\nabla^2[E] + k_b[ES] - k_f[S][E] + k_{cat}[ES] \\
&\quad + k_b^I[EI] - k_f^I[I][E] \\
\frac{\partial[P]}{\partial t} &= k_{cat}[ES] \\
\frac{\partial[I]}{\partial t} &= k_b^I[EI] - k_f^I[I][E] \\
\frac{\partial[EI]}{\partial t} &= k_f^I[I][E] - k_b^I[EI],
\end{aligned} \tag{5}$$

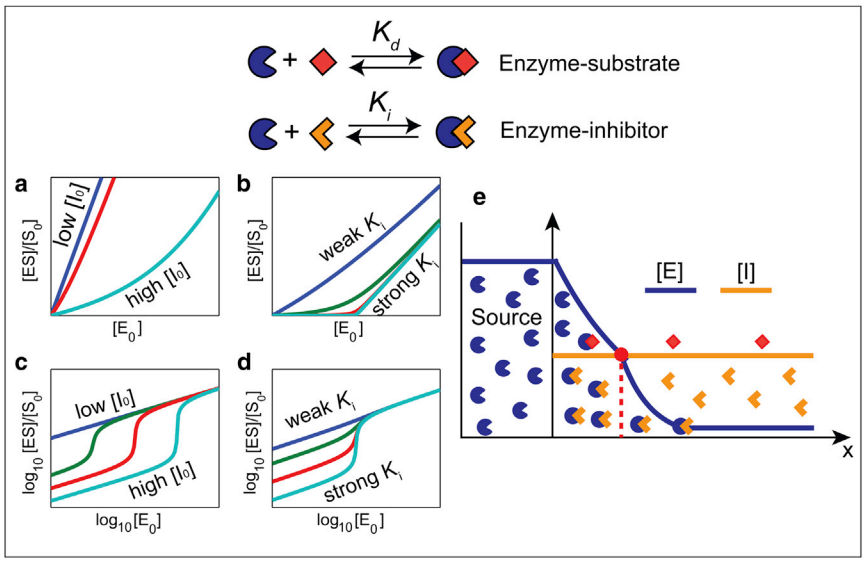

FIGURE 2 Spatial propagation of enzymatic activity modulated by molecular titration. Inhibitor competes with substrate for binding to the active site characterized by the dissociation constant K_i. Steady-state concentrations of enzyme-substrate complex as a function of the total concentration of enzyme were calculated by employing a homogeneous equilibrium model (44). (*a*) Dimensionless steady-state concentration of enzyme-substrate complex, $[ES]/[S_0]$, as a function of total enzyme concentration, $[E_0]$, for various total concentrations of inhibitor, $[I_0]$. In all calculations, the substrate dissociation constant and the inhibitor dissociation constant are $K_d = 4.0 \times 10^{-2}$ M and $K_i = 10^{-9}$ M, respectively. A substrate concentration of 0.1 mg/ml was employed. (*b*) Dimensionless steady-state concentration of enzyme-substrate complex, $[ES]/[S_0]$, as a function of total enzyme concentration, $[E_0]$, for various values of the dissociation constant K_i. In all calculations, $K_d = 4.0 \times 10^{-2}$ M, the inhibitor concentration is 10 μM, and the substrate concentration is 0.1 mg/ml. (*c* and *d*) The same solutions as in *a* and *b* on log-log axes. As can be clearly observed, once the concentration of enzyme equals the inhibitor concentration, a threshold response occurs. The sharpness of the response depends on the ratio K_i/K_d. (*e*) Schematic representation of the effect of molecular titration on spatial propagation of enzymatic activity. When association of enzyme to inhibitor is fast with respect to diffusion, enzyme first fills the covalently bound inhibitor sink in each site before free enzyme is available to convert substrate, resulting in retardation and concomitant sharpening of the product front (vide infra).

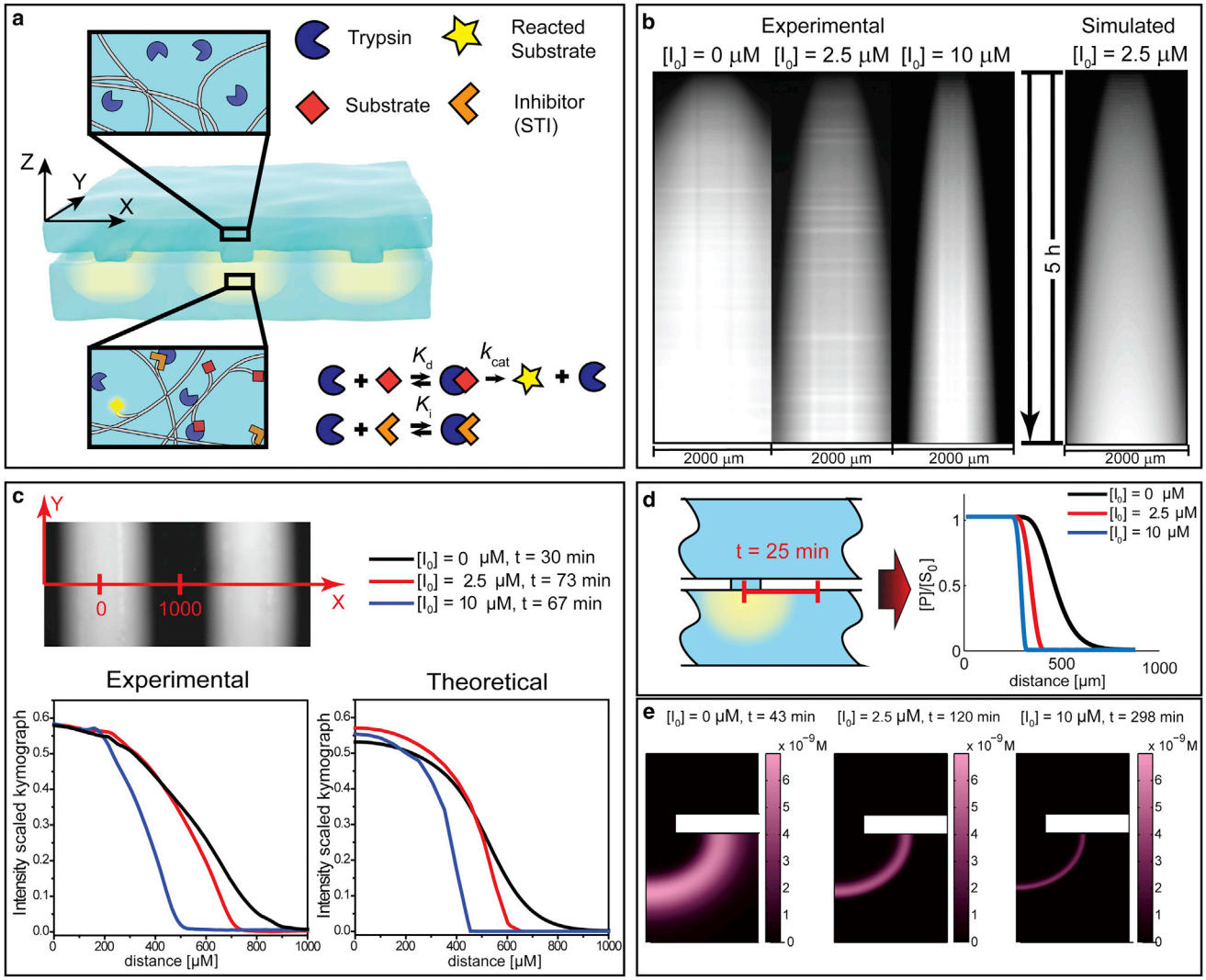

FIGURE 3 Spatial propagation of enzymatic activity in the presence of a strong, cross-linked inhibitor. (*a*) Schematic representation of the wet stamping experiment in which trypsin diffuses into a gel containing cross-linked fluorogenic substrate and STI. STI was treated with N-acryloyl-ε-aminocaproic acid NHS ester and copolymerized with acrylamide together with the fluorogenic substrate. (*b*) Comparison of experimental kymographs for different concentrations of copolymerized STI, $[I_0] = 0$, 2.5, and 10 μM, $[S_0] = 0.1$ mg/ml, and $[E_0] = 2$ mg/ml). A simulated kymograph generated using the set of parameters $[S_0] = 0.1$ mg/ml, $[E_0] = 2$ mg/ml, $[I_0] = 2.5$ μM, $D_e = 1.0 \times 10^{-11}$ m^2 s^{-1}, $k_{cat}/K_d = 4.7 \times 10^2$ s^{-1} M^{-1}, and $K_i = 10^{-9}$ M is shown on the right. The value of k_{cat}/K_d was obtained by nonlinear least-square analysis of the experimental kymograph obtained in the absence of inhibitor. (*c*) Fluorescent product front for different concentrations of cross-linked STI inhibitor, showing an increase in steepness for higher concentrations of inhibitor. The upper image shows the location of the intensity traces drawn in the image. Because spreading of trypsin is delayed in the presence of inhibitor, the profiles are compared at time points of approximately equal kymograph intensity. The experimental and theoretical plots display the intensities obtained from the scaled kymographs. Parameter values used for the simulations are as follows: for $[I_0] = 0$ μM – $D_e = 1.8 \times 10^{-11}$ m^2 s^{-1}, $k_{cat}/K_d = 4.7 \times 10^2$ s^{-1} M^{-1}; for $[I_0] = 2.5$ μM – $D_e = 1.0 \times 10^{-11}$ m^2 s^{-1}, $k_{cat}/K_d = 4.7 \times 10^2$ s^{-1} M^{-1}, and $K_i = 10^{-9}$ M; for $[I_0] = 10$ μM – $D_e = 8.2 \times 10^{-12}$ m^2 s^{-1}, $k_{cat}/K_d = 4.7 \times 10^2$ s^{-1} M^{-1}, and $K_i = 10^{-9}$ M. (*d*) Theoretical substrate conversion profiles at the top of the gel layer for different inhibitor concentrations at time $t = 25$ min. Parameters used in the simulations are identical to those in *c*. (*e*) Influence of the inhibitor concentration on spatial localization of the enzyme-substrate complex. Parameters used are identical to those in *c*. For visualization purposes, the maximum of the concentration scale was set to 7×10^{-9} M.

where k^I_f and k^I_b are the forward and backward rate constants that describe production and dissociation of enzyme-inhibitor (*EI*) complex, because binding of the substrate and inhibitor occurs again on a much faster timescale compared to diffusion of free enzyme, both enzyme-substrate and enzyme-inhibitor binding were modeled by employing a pseudo-steady-state approximation characterized by the dissociation constants K_d and K_i (k^I_b/k^I_f). The system of PDEs was solved on the same geometry using the same boundary conditions as employed before. Comparison of the concentrations obtained from the approximated model with those from the full PDE model (Eq. 5) again shows good correspondence (see Methods). Nonlinear least-square analysis of the experimental kymograph

acquired by wet stamping of trypsin to a PAAm gel containing cross-linked STI ($[I_0] = 2.5\ \mu$M) shows that the computational model correctly describes the influence of inhibitor on spatiotemporal product formation (Fig. 3 *b*). Profile-likelihood analysis reveals that the inhibitor dissociation constant, K_i, is practically unidentifiable but should be $<10^{-7}$ M, in agreement with values reported in the literature (Fig. S8) (47). Further simulations with the computational model reveal that spatial propagation of enzymatic activity is only delayed when binding of inhibitor to the active site of the enzyme is much stronger than binding of the enzyme to its substrate (Fig. S9).

Diffusion of molecules from a restricted source results in smoothening of the gradient in space. Without ultrasensitivity, any downstream signal that arises from enzymatic conversion of this gradient is also spatially smoothened. Our experimental results show that incorporation of strong inhibitors to the PAAm gel sharpens the spatial gradient of enzymatic activity. In the absence of inhibitor, the profile acquired from the kymograph reveals a shallow gradient of enzymatic activity in space, indicative of a graded boundary between regions of high and low converted substrate (Fig. 3 *c*). Simulations with the PDE model, in which the concentration of enzyme-substrate complex are plotted as a function of the total concentration of enzyme at a single point in the PAAm gel, indeed reveal the presence of a critical threshold and steeper curves as the concentration of inhibitor increases, similar to the plots of the nonspatial molecular titration model depicted in Fig. 2 (Fig. S10). As a result of such ultrasensitive and threshold effects, addition of cross-linked inhibitor significantly sharpens the downstream gradient and the steepness of the gradient can be tuned by the total concentration of inhibitor. Comparison of the experimental and computed ($K_i = 10^{-9}$ M) fluorescence intensities again show excellent agreement, and the computational model correctly predicts steeper gradients of enzymatic activity for increasing concentrations of stationary inhibitor (Fig. 3 *d*). When inhibitor and substrate bind with comparable strength, simulations reveal that the concentration increase of product at a single point in the PAAm gel shows sigmoidal kinetics. However, in the ultrasensitive regime, a significant temporal delay is introduced before fluorescent product appears (Fig. S11). Because the boundary between regions of high and low concentrations of converted substrate sharpens in the presence of a strong inhibitor, the width of the traveling wave of enzyme-substrate complex decreases significantly for increasing concentrations of strong inhibitor (Fig. 3 *e* and Fig. S12).

In general, it is expected that free diffusion of inhibitor would broaden the interface between regions of high and low substrate conversion. To understand the interplay between steepness of the product front, diffusion of enzyme and inhibitor, and total concentration of inhibitor, we repeated the wet-stamping experiments using various concentrations of mobile STI ($[E_0] = 1$ mg/ml, $[S_0] = 0.1$ mg/ml) in the PAAm film. As the molecular weights of STI and trypsin are close to each other, their diffusion constants (D_e and D_i) are practically identical. The experimental kymograph obtained using 2.5 μM STI shows that propagation of enzymatic activity is delayed in the presence of a freely diffusing inhibitor (Fig. 4 *a*), comparable to the deceleration observed with cross-linked inhibitor (Fig. 3 *b*). The steepness of the product fronts is also similar, as shown in Fig. 4 *c*, which plots the normalized fluorescent intensity along the x axis at time $t = 120$ min, obtained from the fluorescent micrographs for different concentrations of mobile and stationary inhibitor.

This result clearly indicates that free diffusion of inhibitor does not lead to substantial broadening of the downstream gradient of enzymatic activity. Furthermore, the data show that the steepness of the front can again be tuned by varying the total concentration of mobile inhibitor. In vivo, inhibitors are often small molecules, and therefore, the ratio D_i/D_e deviates from unity, resulting in differential diffusivity of components. We therefore computationally investigated the effect of differential diffusivity of the inhibitor and enzyme in the ultrasensitive regime ($K_i << K_d$) and found that the steepness of the product front is robust to the ratio D_i/D_e (Fig. S13).

Intriguingly, at high concentrations of mobile inhibitor (20 μM), deceleration of the product front is so severe that after some rapid, transient propagation, the product front becomes stationary in space, a phenomenon known as front or wave pinning (49–51). This pinning phenomenon is caused by the continuous influx of free inhibitor to the region of the PAAm gel where substrate conversion was initiated by diffusive transport of the enzyme from the agarose stamp (Fig. 4 *b*). The corresponding computations in Fig. 4 *b* show how propagation of enzymatic activity is effectively blocked by an influx of inhibitor, resulting in a spatial barrier consisting of a high local concentration of enzyme-inhibitor complex, which results in trapping of the wave of enzyme-substrate complex as it emerges from the stamp. It is important to note that the mechanism by which front pinning in this system occurs is fundamentally different from previously considered mechanisms of propagation failure, which find their origin in bistability of the reaction terms as a result of positive feedback (49,51). Simulations with the computational model using an inhibitor dissociation constant of 10^{-9} M ($K_d/K_i \approx 10^7$), in which the effect of total inhibitor concentration and diffusion of the inhibitor on front propagation were assessed (Fig. S14), reveal that front pinning occurs at high concentrations of inhibitor ($\geq 20\ \mu$M) and only when the diffusion constant of the inhibitor is comparable to or larger than the diffusion constant of the enzyme. Kymographs obtained using a smaller value of K_i (10^{-5} M, $K_d/K_i \approx 10^3$) fail to show any evidence of front pinning in a physiologically relevant concentration range ($[I_0] = 0$–$40\ \mu$M; Fig. S15), thus

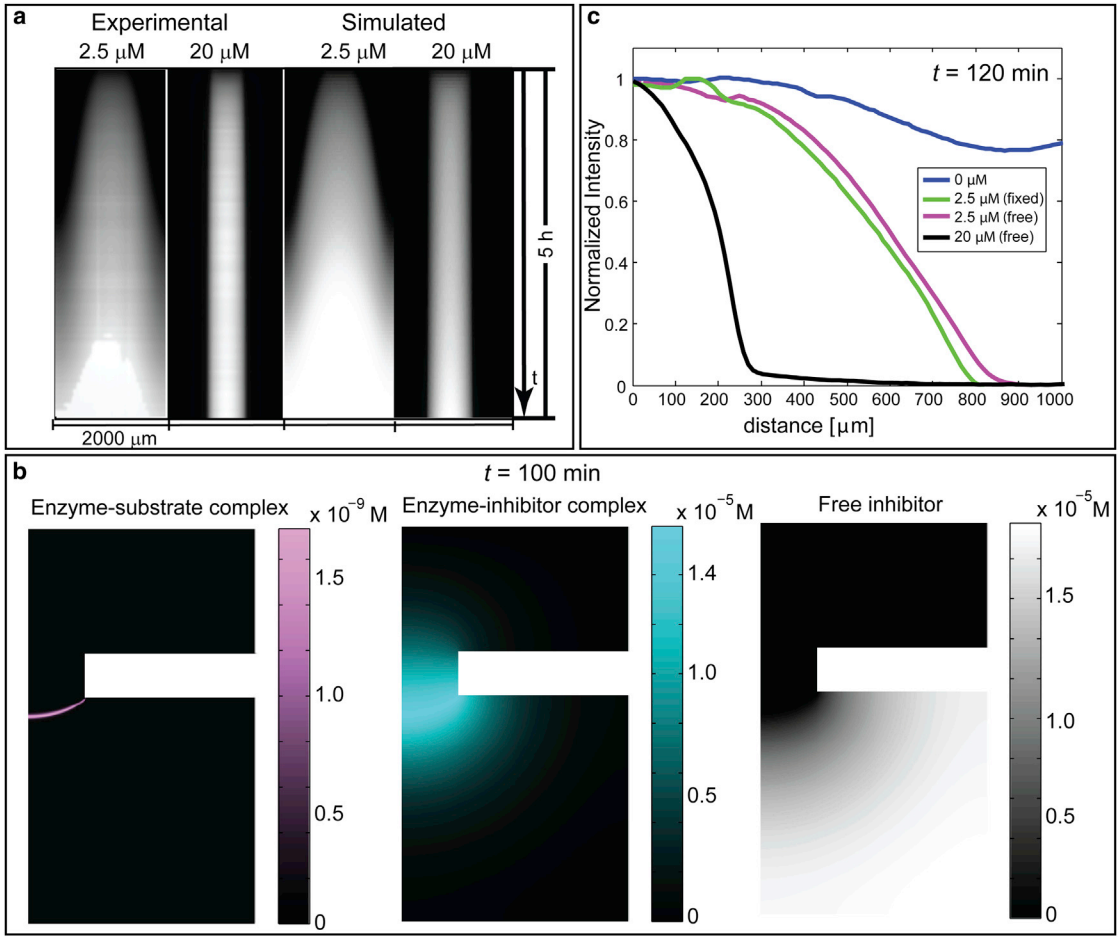

FIGURE 4 Spatial propagation of enzymatic activity in the presence of a strong, mobile inhibitor. (*a*) Comparison of experimental and theoretical kymographs obtained by wet stamping of trypsin to substrate-functionalized PAAm gels soaked in various concentrations of STI ($[S_0] = 0.1$ mg/ml, $[E_0] = 1$ mg/ml). Simulated kymographs were obtained using the parameters $D_e = 1.8 \times 10^{-11}$ m^2 s^{-1}, $k_{cat}/K_d = 4.7 \times 10^2$ s^{-1} M^{-1}, and $K_i = 10^{-9}$ M. The diffusion constants of STI (D_i) and enzyme-STI complex (D_{ei}) used in the simulations are estimated from the Stokes-Einstein relation using the value of D_e. (*b*) Computed concentrations of enzyme-substrate complex (*ES*), enzyme inhibitor complex (*EI*), and free STI (*I*) in the agarose stamp and PAAm gel obtained by simulations using the same parameters as in *a* ($[I_0] = 20$ μM, $[S_0] = 0.1$ mg/ml, and $[E_0] = 1$ mg/ml) at time $t = 100$ min. (*c*) Normalized fluorescent product front at time $t = 120$ min for different concentrations of mobile and stationary STI, showing an increase in steepness of the front in the presence of higher concentrations of mobile inhibitor. The intensities were obtained directly from the fluorescent micrographs and were normalized to the highest value.

indicating the importance of ultrasensitive and threshold effects on propagation failure.

SUMMARY AND CONCLUSION

We have presented an experimental in vitro platform based on diffusion of an enzyme into substrate- and inhibitor-laden gels with the aim to rationalize the role of ultrasensitivity and threshold effects on spatially propagating enzymatic reactions. The ultrasensitive protein switch is engineered by employing the principle of molecular titration using competitive inhibitors with a very high binding strength. A system-level investigation, combining experiments and computations, reveals the influence of various physicochemical parameters and input cues on spatial propagation of enzymatic activity. Molecular titration spatially modulates the shape of a downstream gradient by converting a shallow gradient originating from a localized source into a steep gradient of enzymatic activity. Because the threshold level can be easily tuned by varying the concentration of inhibitor, the positional information of a downstream gradient can be actively controlled in vivo. Our results could provide important insights into the spatial partitioning of transcriptional (52) and nontranscriptional (35,53) regulation of gene expression for which recent work has shown the importance of ultrasensitivity by molecular titration.

Finally, the modularity of our experimental in vitro platform allows for the introduction of a wide variety of biochemical reactions that can further tune the positional information of a downstream gradient. For example, by

addition of autocatalytic enzymatic reactions or by applying mechanical force to the PAAm hydrogel, the platform can be used to experimentally verify current hypotheses on gradient scaling (21,54) or assess the importance of mechanochemical feedback mechanisms (55). Looking beyond the in vitro study of biochemical networks, we also envisage the importance of ultrasensitivity in materials science, where recent efforts have shown the possibility of engineering autonomous materials capable of mechanical synchronization by coupling of diffusion and chemomechanical feedback loops (56–59).

SUPPORTING MATERIAL

Eighteen figures, two tables, references (60–67), and Supporting Methods are available at http://www.biophysj.org/biophysj/supplemental/S0006-3495(13)00781-9.

REFERENCES

1. Mukherji, S., and A. van Oudenaarden. 2009. Synthetic biology: understanding biological design from synthetic circuits. *Nat. Rev. Genet.* 10:859–871.
2. Khalil, A. S., and J. J. Collins. 2010. Synthetic biology: applications come of age. *Nat. Rev. Genet.* 11:367–379.
3. Bashor, C. J., A. A. Horwitz, …, W. A. Lim. 2010. Rewiring cells: synthetic biology as a tool to interrogate the organizational principles of living systems. *Annu. Rev. Biophys.* 39:515–537.
4. Liu, A. P., and D. A. Fletcher. 2009. Biology under construction: in vitro reconstitution of cellular function. *Nat. Rev. Mol. Cell Biol.* 10:644–650.
5. Schwille, P., and S. Diez. 2009. Synthetic biology of minimal systems. *Crit. Rev. Biochem. Mol. Biol.* 44:223–242.
6. Forster, A. C., and G. M. Church. 2007. Synthetic biology projects in vitro. *Genome Res.* 17:1–6.
7. Simpson, M. L. 2006. Cell-free synthetic biology: a bottom-up approach to discovery by design. *Mol. Syst. Biol.* 2:1–2.
8. Hockenberry, A. J., and M. C. Jewett. 2012. Synthetic in vitro circuits. *Curr. Opin. Chem. Biol.* 16:253–259.
9. Kim, J., K. S. White, and E. Winfree. 2006. Construction of an in vitro bistable circuit from synthetic transcriptional switches. *Mol. Syst. Biol.* 2:1–12.
10. Padirac, A., T. Fujii, and Y. Rondelez. 2012. Bottom-up construction of in vitro switchable memories. *Proc. Natl. Acad. Sci. USA.* 109:E3212–E3220.
11. Kim, J., and E. Winfree. 2011. Synthetic in vitro transcriptional oscillators. *Mol. Syst. Biol.* 7:1–15.
12. Montagne, K., R. Plasson, …, Y. Rondelez. 2011. Programming an in vitro DNA oscillator using a molecular networking strategy. *Mol. Syst. Biol.* 7:1–7.
13. Nakajima, M., K. Imai, …, T. Kondo. 2005. Reconstitution of circadian oscillation of cyanobacterial KaiC phosphorylation in vitro. *Science.* 308:414–415.
14. Loose, M., E. Fischer-Friedrich, …, P. Schwille. 2008. Spatial regulators for bacterial cell division self-organize into surface waves in vitro. *Science.* 320:789–792.
15. Ivanov, V., and K. Mizuuchi. 2010. Multiple modes of interconverting dynamic pattern formation by bacterial cell division proteins. *Proc. Natl. Acad. Sci. USA.* 107:8071–8078.
16. Míguez, D. G., V. K. Vanag, and I. R. Epstein. 2007. Fronts and pulses in an enzymatic reaction catalyzed by glucose oxidase. *Proc. Natl. Acad. Sci. USA.* 104:6992–6997.
17. Liao, X., R. T. Petty, and M. Mrksich. 2011. A spatially propagating biochemical reaction. *Angew. Chem. Int. Ed. Engl.* 50:706–708.
18. Karsenti, E. 2008. Self-organization in cell biology: a brief history. *Nat. Rev. Mol. Cell Biol.* 9:255–262.
19. Soh, S., M. Byrska, …, B. A. Grzybowski. 2010. Reaction-diffusion systems in intracellular molecular transport and control. *Angew. Chem. Int. Ed. Engl.* 49:4170–4198.
20. Kicheva, A., M. Cohen, and J. Briscoe. 2012. Developmental pattern formation: insights from physics and biology. *Science.* 338:210–212.
21. Lander, A. D. 2011. Pattern, growth, and control. *Cell.* 144:955–969.
22. Neves, S. R., P. Tsokas, …, R. Iyengar. 2008. Cell shape and negative links in regulatory motifs together control spatial information flow in signaling networks. *Cell.* 133:666–680.
23. Brandman, O., and T. Meyer. 2008. Feedback loops shape cellular signals in space and time. *Science.* 322:390–395.
24. Wagner, J., and J. Keizer. 1994. Effects of rapid buffers on Ca^{2+} diffusion and Ca^{2+} oscillations. *Biophys. J.* 67:447–456.
25. Lipshtat, A., G. Jayaraman, …, R. Iyengar. 2010. Design of versatile biochemical switches that respond to amplitude, duration, and spatial cues. *Proc. Natl. Acad. Sci. USA.* 107:1247–1252.
26. McCarrey, J. R., and A. D. Riggs. 1986. Determinator-inhibitor pairs as a mechanism for threshold setting in development: a possible function for pseudogenes. *Proc. Natl. Acad. Sci. USA.* 83:679–683.
27. Hill, T. L. 1985. Cooperativity Theory in Biochemistry. Springer-Verlag, New York.
28. Goldbeter, A., and D. E. Koshland, Jr. 1981. An amplified sensitivity arising from covalent modification in biological systems. *Proc. Natl. Acad. Sci. USA.* 78:6840–6844.
29. Berg, O. G., J. Paulsson, and M. Ehrenberg. 2000. Fluctuations and quality of control in biological cells: zero-order ultrasensitivity reinvestigated. *Biophys. J.* 79:1228–1236.
30. Buchler, N. E., and M. Louis. 2008. Molecular titration and ultrasensitivity in regulatory networks. *J. Mol. Biol.* 384:1106–1119.
31. Kim, S. Y., and J. E. Ferrell, Jr. 2007. Substrate competition as a source of ultrasensitivity in the inactivation of Wee1. *Cell.* 128:1133–1145.
32. Liu, X., L. Bardwell, and Q. Nie. 2010. A combination of multisite phosphorylation and substrate sequestration produces switchlike responses. *Biophys. J.* 98:1396–1407.
33. Melen, G. J., S. Levy, …, B.-Z. Shilo. 2005. Threshold responses to morphogen gradients by zero-order ultrasensitivity. *Mol. Syst. Biol.* 1:1–11.
34. Levine, E., P. McHale, and H. Levine. 2007. Small regulatory RNAs may sharpen spatial expression patterns. *PLOS Comput. Biol.* 3:e233.
35. Mukherji, S., M. S. Ebert, …, A. van Oudenaarden. 2011. MicroRNAs can generate thresholds in target gene expression. *Nat. Genet.* 43: 854–859.
36. Wei, Y., P. J. Wesson, …, B. A. Grzybowski. 2010. Measurement of protein-ligand binding constants from reaction-diffusion concentration profiles. *Anal. Chem.* 82:8780–8784.
37. Wang, Z.-X. 1995. An exact mathematical expression for describing competitive binding of two different ligands to a protein molecule. *FEBS Lett.* 360:111–114.
38. Dixon, M., and E. C. Webb. 1979. Enzymes, 3rd ed. Academic Press, New York.
39. Press, W. H., B. P. Flannery, …, W. T. Vetterling. 2002. Numerical Recipes in C: The Art of Scientific Computing. Cambridge University Press, Cambridge, United Kingdom.
40. Bode, W., and R. Huber. 1992. Natural protein proteinase inhibitors and their interaction with proteinases. *Eur. J. Biochem.* 204:433–451.
41. Leytus, S. P., L. L. Melhado, and W. F. Mangel. 1983. Rhodamine-based compounds as fluorogenic substrates for serine proteinases. *Biochem. J.* 209:299–307.

42. Erlanger, B. F., N. Kokowsky, and W. Cohen. 1961. The preparation and properties of two new chromogenic substrates of trypsin. *Arch. Biochem. Biophys.* 95:271–278.

43. Gabel, D., and V. Kasche. 1972. Cooperative transitions between active α- and β-trypsin conformations. *Biochem. Biophys. Res. Commun.* 48:1011–1018.

44. Klajn, R., M. Fialkowski, …, B. A. Grzybowski. 2004. Multicolour micropatterning of thin films of dry gels. *Nat. Mater.* 3:729–735.

45. Raue, A., C. Kreutz, …, J. Timmer. 2009. Structural and practical identifiability analysis of partially observed dynamical models by exploiting the profile likelihood. *Bioinformatics.* 25:1923–1929.

46. Laskowski, M., and M. Laskowski, Jr. 1954. Naturally occurring trypsin inhibitors. *Adv. Protein Chem.* 9:203–242.

47. Luthy, J. A., M. Praissman, …, M. Laskowski. 1973. Detailed mechanism of interaction of bovine β-trypsin with soybean trypsin inhibitor (Kunitz). I. Stopped flow measurements. *J. Biol. Chem.* 248:1760–1771.

48. Lebowitz, J., and M. Laskowski. 1962. Potentiometric measurment of protein-protein association constants. Soybean trypsin inhibitor-trypsin association. *Biochemistry.* 1:1044–1055.

49. Mori, Y., A. Jilkine, and L. Edelstein-Keshet. 2008. Wave-pinning and cell polarity from a bistable reaction-diffusion system. *Biophys. J.* 94:3684–3697.

50. Keitt, T. H., M. A. Lewis, and R. D. Holt. 2001. Allee effects, invasion pinning, and species' borders. *Am. Nat.* 157:203–216.

51. Laplante, J. P., and T. Erneux. 1992. Propagation failure and multiple steady states in an array of diffusion coupled flow reactors. *Physica A.* 188:89–98.

52. Lee, T.-H., and N. Maheshri. 2012. A regulatory role for repeated decoy transcription factor binding sites in target gene expression. *Mol. Syst. Biol.* 8:1–11.

53. Ray, J. C. J., J. J. Tabor, and O. A. Igoshin. 2011. Non-transcriptional regulatory processes shape transcriptional network dynamics. *Nat. Rev. Microbiol.* 9:817–828.

54. Ben-Zvi, D., B.-Z. Shilo, and N. Barkai. 2011. Scaling of morphogen gradients. *Curr. Opin. Genet. Dev.* 21:704–710.

55. Howard, J., S. W. Grill, and J. S. Bois. 2011. Turing's next steps: the mechanochemical basis of morphogenesis. *Nat. Rev. Mol. Cell Biol.* 12:392–398.

56. He, X., M. Aizenberg, …, J. Aizenberg. 2012. Synthetic homeostatic materials with chemo-mechano-chemical self-regulation. *Nature.* 487:214–218.

57. Jakobus, K., S. Wend, and W. Weber. 2012. Synthetic mammalian gene networks as a blueprint for the design of interactive biohybrid materials. *Chem. Soc. Rev.* 41:1000–1018.

58. Yoshida, R. 2011. Self-oscillating polymer gel as novel biomimetic materials exhibiting spatiotemporal structure. *Colloid Polym. Sci.* 289:475–487.

59. Kolmakov, G. V., V. V. Yashin, …, A. C. Balazs. 2010. Designing communicating colonies of biomimetic microcapsules. *Proc. Natl. Acad. Sci. USA.* 107:12417–12422.

60. Ioffe, I. S., and V. F. Otten. 1961. Investigations in field of rhodamine dyestuffs and compounds related to them. 1. Parent substance of rhodamines, its preparation and properties. *Zh. Obshch. Khim.* 31:1511–1517.

61. Lavis, L. D., T. Y. Chao, and R. T. Raines. 2006. Fluorogenic label for biomolecular imaging. *ACS Chem. Biol.* 1:252–260.

62. Chung, I. D., P. Britt, …, J. Mays. 2005. Synthesis of amino acid-based polymers via atom transfer radical polymerization in aqueous media at ambient temperature. *Chem. Commun.* (*Camb.*). (8):1046–1048.

63. Zheng, Y., C. Duanmu, and Y. Gao. 2006. A magnetic biomimetic nanocatalyst for cleaving phosphoester and carboxylic ester bonds under mild conditions. *Org. Lett.* 8:3215–3217.

64. Auernheimer, J., C. Dahmen, …, H. Kessler. 2005. Photoswitched cell adhesion on surfaces with RGD peptides. *J. Am. Chem. Soc.* 127:16107–16110.

65. Murphy, S., and A. van der Vaart. 2000. On Profile Likelihood. *J. Am. Stat. Assoc.* 95:449–485.

66. Amsden, B. 1998. Solute diffusion within hydrogels: mechanisms and models. *Macromolecules.* 31:8382–8395.

67. Kaiser, P. M. 1980. Substrate inhibition as a problem of non-linear steady state kinetics with monomeric enzymes. *J. Mol. Catal.* 8: 431–442.